International Journal of Hydrogen Energy 230 (2026) 154773

Contents lists available at ScienceDirect

International Journal of Hydrogen Energy

journal homepage: www.elsevier.com/locate/he

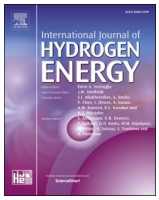

Comparative risk analysis of aqueous formate solutions and compressed hydrogen storage: Safety and scalability assessment

Fabrizio Di Franco, Danilo Russo *, Almerinda di Benedetto

Dipartimento di Ingegneria Chimica, dei Materiali e della Produzione Industriale, Università degli Studi di Napoli Federico II, Naples, Italy

ARTICLE INFO

Keywords:
Hydrogen storage
Formate
Inherent safety
Industrial scalability
Risk assessment

ABSTRACT

This work investigates the safety performance of low-pressure aqueous formate solutions as an alternative hydrogen storage strategy, comparing them with conventional high-pressure compressed hydrogen tanks. Quantitative consequence analyses were performed using PHAST 9.0, considering both continuous and catastrophic release scenarios across a wide range of vessel volumes and operating pressures. The results show that aqueous systems exhibit markedly reduced hazard distances in dispersion, jet fire, fireball, and explosion events, primarily due to the dilution effect of water vapor, which lowers the calorific value and radiant efficiency of hydrogen, and lower release pressure. In particular, the 50% fatality threshold was never reached for aqueous storage cases, while compressed hydrogen consistently produced severe consequences that scaled with vessel size. Moreover, volume scale-up of aqueous formate tanks displayed a saturation trend, indicating increasing industrial scalability without proportional escalation of risk. Furthermore, in accidental release scenarios at near-ambient temperature and pressure, hydrogen generation is kinetically limited and concentrations remain below the lower flammability limit, confirming intrinsically safe behavior under normal operating conditions. These findings highlight the inherent safety advantages of aqueous formate solutions, supporting their potential as safer hydrogen carriers for large-scale applications.

1. Introduction

The rising global energy demand represents a major challenge for modern society [1]. Driven by the continuous population growth, annual energy consumption has increased dramatically, from 5×10^{12} kWh in 1860 to 1.2×10^{14} kWh today [2]. According to the International Energy Agency (IEA), global energy demand is expected to double by 2030 [3]. Unless significant technological advances or regulatory measures are implemented, this trend will result in a further increase in oil and natural gas consumption, which remain the dominant energy carriers. At present, fossil fuels account for 80–85% of global energy use [4].

This reliance is unsustainable not only because of resource depletion but also due to severe environmental impacts. Each year, approximately 41 Gt of CO_2 are emitted into the atmosphere [5], contributing to global warming, glacier retreat, and phenomena such as acid rain [6].

To address these challenges, hydrogen has emerged as a promising alternative energy carrier [7]. Interest in hydrogen as a fuel dates back to the 1974 energy crisis [8]. However, since hydrogen is not naturally available, it must be produced from hydrogen-rich compounds. Conventional production methods include steam methane reforming, partial oxidation, autothermal reforming, and hydrocarbon pyrolysis [9]. Yet, because of their large CO_2 footprint, alternative renewable-based routes, such as biomass conversion and water splitting, are under active investigation [10–13]. Hydrogen offers clear advantages: (i) high gravimetric energy density (120 MJ kg^{-1}) [14], about three times that of gasoline; (ii) excellent conversion efficiency in fuel cells [11]; (iii) absence of CO_2 emissions at the point of use, where only water is generated [15]. Despite these benefits, large-scale deployment faces several barriers, particularly the development of efficient renewable production methods, the establishment of supply infrastructures, and safe storage solutions [16–19]. To increase volumetric energy density, hydrogen is mainly stored either as compressed gas at high pressure (350–700 bar) or as a cryogenic liquid (21.2 K) [20]. While both methods are commercially mature, they present significant safety challenges: more than 270 incidents of hydrogen release have been documented [21]. This stems from hydrogen intrinsic properties, i.e. [22] very low ignition energy (0.02 mJ), wide flammability range (4–75

* Corresponding author.
E-mail address: danilo.russo3@unina.it (D. Russo).

https://doi.org/10.1016/j.ijhydene.2026.154773
Received 20 January 2026; Received in revised form 5 March 2026; Accepted 27 March 2026
Available online 4 April 2026

mol% in air), and high diffusivity. Research on hydrogen energy storage systems (HESS) has primarily focused on economic aspects, often overlooking safety. For instance, Arsad et al. [23] reported that among nearly 10000 publications on HESS, 82.5% of the most cited works emphasize economic performance rather than safety considerations [24]. Economic viability can indeed be improved by optimizing storage capacity and operating strategies, but comprehensive assessment must also integrate hazard evaluation [24]. Although safety is often cited as a major concern in the path toward commercialization and wider adoption of hydrogen-based storage solutions, there is still a lack of in-depth, systematic studies specifically focused on evaluating the associated risks [25–27]. Despite the gaps in the current literature, there are several practical examples of Quantitative Risk Assessment (QRA) involving hydrogen release, which highlight the severity of the consequences as tank volumes increase from laboratory to industrial scale [25,28–36]. Dadashzadeh et al. [34] quantified the risks associated with onboard hydrogen storage during fire scenarios. The main objective is to estimate the risk in terms of human losses, using two indicators: the cost in human lives per fire event and the annual fatality rate per vehicle. To achieve this, the authors combine an analysis of the physical consequences of the accident with the likelihood of their occurrence. The consequences considered include the formation of blast waves and fireballs caused by the rupture of the hydrogen tank. Kim et al. [35] developed a quantitative model for assessing the risk associated with hydrogen infrastructure, such as production plants, storage systems, and transport networks. The central idea is to construct a numerical index that enables the comparison of different configurations in terms of safety, accounting for both the intrinsic risk of the technology employed and the environmental context. On one hand, the technical risk of each unit is evaluated through a classification of potential failures; on the other, an environmental factor is introduced, which considers how vulnerable a given area would be in the event of an accident. This model allows for the calculation of an overall risk index for the entire infrastructure by aggregating the contributions from each stage: production, storage, and transportation. Furthermore, tools such as HyRAM have been increasingly employed for quantitative risk assessment (QRA), enabling simulations of gas leaks, jet fires, and explosions. [33]. Besides compressed or cryogenic hydrogen, a wide range of alternative hydrogen storage strategies has been investigated in recent years, including metal hydrides [37,38], liquid organic hydrogen carriers (LOHCs) [39–41], metal–organic frameworks (MOFs) [42,43], and porous adsorbent materials [44,45]. Metal hydrides [46,47] can achieve high volumetric hydrogen densities and operate at relatively low pressures; however, they are often characterized by slow hydrogen absorption/desorption kinetics, significant heat management requirements due to the endothermic/exothermic nature of the reactions, and potential material degradation over repeated cycles. LOHC systems offer the advantage of liquid-phase handling and compatibility with existing fuel infrastructures, but typically require elevated temperatures and catalytic reactors for hydrogen release, with associated energy penalties and safety considerations. Physisorption-based systems, such as MOFs and other porous adsorbents, enable reversible hydrogen storage under mild conditions and allow for tunable material properties; nevertheless, their practical application is often limited by low working capacities at ambient temperature and the need for cryogenic or moderately pressurized operation. Overall, while these approaches address some of the limitations of conventional hydrogen storage, each technology introduces specific constraints related to kinetics, thermodynamics, and system-level integration that must be carefully accounted for in safety and risk assessments.

As an alternative, hydrogen can be stored in aqueous formate solutions. In the presence of noble-metal-based catalysts, hydrogen can be released under mild operating conditions (323–363 K, 2–10 bar), with simultaneous formation of bicarbonate [48–50]. Moreover, the process is reversible: bicarbonate can be reconverted to formate at higher hydrogen pressures.

$$MCOOH + H_2O \leftrightarrow MHCO_3 + H_2 \quad \text{Eq.1}$$

Where $M = Na^+, K^+, NH_4^+$ is the counterion. This method is inherently safer because of the moderate operating conditions and the mitigating effect of water. This study focuses on aqueous formates, with compressed hydrogen used as a benchmark due to its technological maturity. Other hydrogen storage approaches, such as metal hydrides, liquids, MOFs, or adsorbents, are mentioned to provide broader context, but their detailed analysis is beyond the scope of the present work. Nevertheless, potential accident scenarios involving aqueous formates must still be assessed. Russo et al. analyzed hydrogen releases and ignition from tanks in the presence of an external fire under two different scenarios: (i) safety valve activation, resulting in a hydrogen-only release, and (ii) valve failure with catastrophic tank rupture, leading to a hydrogen-water vapor cloud [51]. Their findings indicated that for a 200 L tank, aqueous formate consistently presented lower risks than high-pressure hydrogen storage, regardless of operating pressure. [51]. Building on this work, the present study extends the consequence analysis by considering larger tank volumes representative of industrial applications [51]. Semi-empirical models are replaced by detailed simulations using PHAST 9.0, a software increasingly adopted in hydrogen safety studies for modeling gas dispersion, ignition, and explosion scenarios [29]. Here, volumes from 0.5 to 5 m^3 are analyzed to assess the safety performance of aqueous formate storage at industrial scale. The use of PHAST enables realistic consequence modelling and provides a robust framework for evaluation hydrogen storage alternatives.

2. Methods

The methodological framework adopted in this work combines time-scale analysis and consequence modeling to assess hydrogen release behavior under both normal and accidental conditions. The time-scale analysis provides a physically grounded criterion to distinguish kinetic- and discharge-controlled regimes, while consequence analysis quantifies the associated hazard distances in terms of dispersion, thermal radiation, and overpressure. This integrated approach enables a consistent comparison between aqueous formate-based storage and conventional compressed hydrogen systems. In the simulated accidental scenarios, storage tanks containing aqueous formate solutions were compared with conventional high-pressure tanks (P = 350 bar). The two systems were designed to contain the same overall quantity of hydrogen. Five aqueous formate storage cases were analyzed, corresponding to set-pressures of the safety valve of 10, 20, 30, 40, and 50 bar, in addition to the reference high-pressure hydrogen storage case. The simulations assumed exposure to an external fire as the triggering event.

As highlighted by Makridis [52], compressed hydrogen significantly deviates from ideal gas behavior, unlike most other gases. Specifically, at high pressures, hydrogen occupies a larger volume than predicted by the ideal gas law. This deviation is accounted for by introducing the compressibility factor (Z) into the equation of state [53]:

$$PV = nZRT, \text{where } Z = \frac{n_{ideal}}{n_{real}} = \frac{m_{ideal}}{m_{real}} \quad \text{Eq.2}$$

At ambient temperature and 350 bar, the compressibility factor for hydrogen is approximately 1.2, which was adopted in all subsequent calculations.

The consequence analysis was performed using the PHAST 9.0 software package. PHAST was used as an industry-standard tool to perform a consistent and conservative comparative consequence analysis between aqueous formate and high-pressure hydrogen storage systems. While detailed hydrogen–steam multiphase hydrodynamics are not explicitly resolved, the multi-component framework captures the dominant macroscopic effects relevant for safety assessment, including hydrogen dilution by steam and attenuation of thermal radiation and overpressure. Conservative assumptions were adopted to ensure upper-

Table 1
Atmospheric conditions used in PHAST simulations.

	Properties	Values
Weather	Wind Speed (m/s)	2
	Pasquill Stability	F – moderately stable
	Atmospheric Temperature (°C)	25
	Relative Humidity (fraction)	0.7
	Solar Radiation Flux (kW/m^2)	0.5

Table 2
Main input parameters for catastrophic rupture simulations in PHAST.

Parameter	Value	Notes
Material	H_2, H_2+H_2O	Pure hydrogen or aqueous formate mixture
Fluid State	Vapor/Two-phase	Depending on tank content
Temperature (°C)	25	Reference condition
Pressure (bar)	$2P_{set}$	Tank pressures analyzed
Mass Inventory	Variable	Calculated via Eq. 2-Eq. 3
Mixture modeling	MC with single aerosol	For Two-phase systems
Expansion method	DNV recommended	Default if no rainout
Terrain	Land	Standard assumption
Explosion method	TNT	Conservative estimation
TNT efficiency	4.6%	Based on Han et al. [54]
Burst type	Air burst	Standard assumption
Radiation levels (kW/m^2)	4, 12.5, 37.5	Standard damage thresholds
Lethality level	0.5 (50%)	For fatalities estimation
Fireball model	Martinsen time-varying	Default
Burst pressure	$2P_{set}$	Critical rupture
Fireball emissive power	700 kW/m^2	Default

bound hazard estimates, in line with the objectives of this study. The main variable parameter was the tank volume, which was increased in steps of 0.5 m^3, from 0.5 m^3 up to 5 m^3, to reproduce release conditions representative of industrial-scale storage systems.

The sizing of aqueous formate tanks depends on the filling level (δ), fixed at 80%, and the concentration of the formate salt (C_{salt}). The total tank volume can be calculated as:

$$V_{tot}(L) = \frac{1}{\delta}\frac{n_{H_2}}{C_{salt}} \quad \text{Eq.3}$$

where n_{H_2} are the moles of hydrogen stored. Each tank was equipped with a 20 mm safety valve positioned on the upper head. Two accident scenarios were considered:

1. *Valve operation:* due to the external fire, the tank temperature rises, enhancing catalytic hydrogen production and partial water vaporization. The pressure increases until reaching the set pressure P_{set}, at which point the safety valve opens. In this case, the contribution of water vapor to the gas phase is negligible, and the release consists almost entirely of hydrogen, modeled as a continuous discharge.
2. *Valve failure:* if the safety valve malfunctions, pressure continues to build until the rupture pressure P_{burst} is reached. This condition, assumed as $2P_{set}$, corresponds to catastrophic tank rupture. The event leads to an instantaneous release of a two-phase hydrogen–-water vapor cloud. A conservative burst pressure of $P_{burst} = 2\,P_{set}$ was assumed for consequence analysis, slightly exceeding typical ASME Section VIII limits (UG-154) to provide an upper-bound estimate.

In PHAST, the *time-varying leak* event type was employed for continuous releases, as it accounts for the evolving thermodynamic conditions inside the tank and the depletion rate. For catastrophic ruptures, the instantaneous release option was selected.

Table 3
Main input parameters for continuous release simulations in PHAST.

Parameter	Value	Notes
Material	H_2	Pure hydrogen
Fluid State	Vapor	-
Temperature (°C)	25	Reference condition
Pressure (bar)	10, 20, 30, 40, 50, 350	Tank pressures analyzed
Mass Inventory	Variable	Calculated by Eq. 2-Eq. 3
Modelling approach	PC modelling	Pure component assumption
Orifice diameter (mm)	20	Representative leak size
Release direction	Horizontal	As modeled
Release elevation	0 m	Ground level
Expansion method	DNV recommended	Default if no rainout
Terrain	Land	Standard assumption
Safety system	None	No blowdown modeled
Jet fire method	DNV recommended	Cone model default
Radiation levels (kW/m^2)	4, 12.5, 37.5	PHAST thresholds
Lethality level	0.5 (50%)	For effect zone estimation
Rate modification factor	3	PHAST default
Jet-fire max *exposure duration (s)*	20	Typical human reaction time [55]

Atmospheric conditions were fixed to represent moderately stable weather, consistent with a Pasquill class F stability, a wind speed of 2 m/s, ambient temperature of 25 °C, relative humidity of 0.7, and solar radiation flux of 0.5 kW/m^2. Simulations were conducted using conservative meteorological conditions (low wind, stable atmosphere). A summary is reported in Table 1.

Specific input parameters were defined for each of the two scenarios.

a. In the case of instantaneous release, six pressure vessels, each corresponding to one of the selected P_{set} values, were configured in PHAST using the Pressure Vessel option with the event type Catastrophic Rupture. For vessels containing aqueous formate solutions, the Multi-Component (MC) with single aerosol option was selected to represent the coexistence of liquid and vapor phases. Explosion effects were modeled using the TNT equivalence method, which provides conservative estimates. Following Han et al. [54], a TNT efficiency factor of 4.6% was adopted, derived from combined experimental–computational analysis of hydrogen vessel bursts. Burst pressure was defined as $P_{burst} = 2P_{set}$, representing critical tank failure under fire exposure. Key modeling parameters for catastrophic rupture simulations are summarized in Table 2.
b. Similarly, in the case of continuous release six pressure vessels with different P_{set} values were modeled as *time-varying leaks*. In this case, a 20 mm orifice diameter was assumed to represent a realistic round-hole release. Other parameters were configured consistently with PHAST default or literature-recommended values, including jet fire modeling, radiation thresholds, and exposure times. A full overview of the adopted parameters is reported in Table 3.

The frequency of occurrence of the outcomes was estimated according to literature guidelines, using the results of a previously reported event tree analysis [51]. The probability of immediate ignition was assumed to vary linearly with the water concentration in the released solution.

3. Results and discussion

3.1. Time scale analysis

In order to determine whether, over the same time window required for tank emptying though the discharge system, the catalytic production rate could reach values comparable to the physical outflow rate from the vessel, we compared the time of generation of hydrogen with the discharge time. To evaluate the hydrogen production time, the experimental results by Dong et al. [56] on bimetallic catalysts were adopted

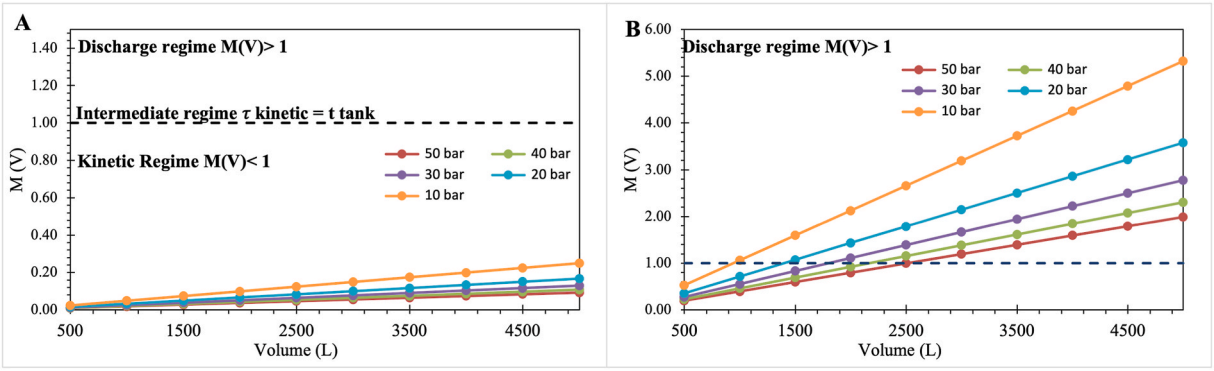

Fig. 1. Dimensionless number. Trend of $M(V) = t_{tank}(V)/\tau_{kinetic}$ as a function of volume for different P_{set} estimated under normal operating conditions (T = 80 °C) (A), and extrapolated at 200 °C (B). The dotted line (—) at $M = 1$ indicates parity between characteristic times; values $M < 1$ denote faster emptying of kinetic production.

as a reference. Under the investigated conditions (80 °C, 1 M ammonium formate) their results support the approximation of the dehydrogenation kinetics by a pseudo-first-order model. On this basis, the characteristic reaction time for 90% conversion was calculated as $\tau_{kinetic} = 6900$ s. To compare the characteristic time of hydrogen release with the tank emptying time, the following dimensionless number M(V) was introduced:

$$M(V) = \frac{t_{tank}(V)}{\tau_{kinetic}} \quad \text{Eq. 4}$$

where $t_{tank}(V)$ is the time required to discharge a storage vessel of volume V.

Based on the value of M(V), three regimes can be identified.

A) Kinetic regime ($M(V) < 1$): hydrogen release is controlled by reaction kinetics, and tank emptying proceeds faster than catalytic hydrogen generation.
B) Intermediate regime ($M(V) = 1$): tank emptying and catalytic hydrogen generation occur on comparable time scales.
C) Discharge-controlled regime ($M(V) > 1$): hydrogen generation is faster than physical discharge, and the release is controlled by the discharge system.

Fig. 1A reports the estimated values of M(V) under normal operating conditions (Tc ≈ 80 °C) as a function of the storage vessel volume for different set-point pressures.

Under all the conditions considered, $M(V)$ remains well below unity across the entire volume range. Even the most conservative case (10 bar set-point pressure), $M(V)$ does not exceed 0.25 at the maximum volume analyzed, while higher set-point pressures have larger margins.

These results indicate that, under normal operating conditions, hydrogen release occurs in Regime A, where kinetic limitations prevent catalytic hydrogen generation from competing with physical discharge. This behavior supports the intrinsically safer nature of aqueous formate-based hydrogen storage during standard operations. To further substantiate this conclusion, an additional accidental release scenario representative of normal operating conditions was analyzed. Specifically, the formation of a hole in the storage vessel was assumed, leading to hydrogen release at near-ambient temperature and pressure in the absence of any external fire. Dispersion calculations performed under these conditions (Fig. S1, Supplementary Material) show that, even in the worse-case scenario (i.e., largest storage vessel volume and negligible water vapor fraction), hydrogen concentrations at ground level never exceed the lower flammability limit (LFL). This confirms that, in the absence of thermal escalation, hydrogen release remains kinetically limited and intrinsically safe (Scenario A1).

Under external fire scenarios, however, temperatures are expected to rise well above 200 °C, leading to a dramatic acceleration of the dehydrogenation reaction. By extrapolating the reported temperature dependence of the reaction kinetics, the characteristic reaction time at 200 °C was estimated as $\tau_{kinetic} = 324$ s. The corresponding values of M (V) are shown in Fig. 1B, at different values of the set pressure. At temperatures higher than 200 °C, hydrogen generation from the solution is expected to be faster than physical discharge through the safety valves

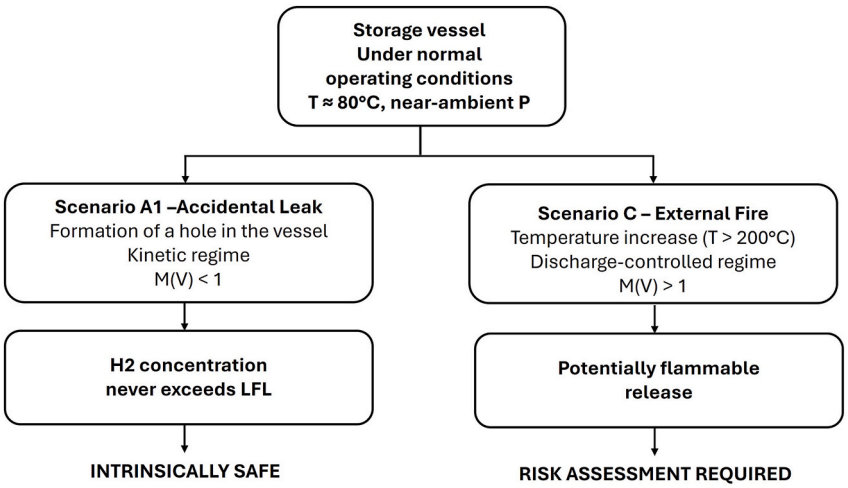

Fig. 2. Flowchart of hydrogen release regimes from aqueous formate storage vessels.

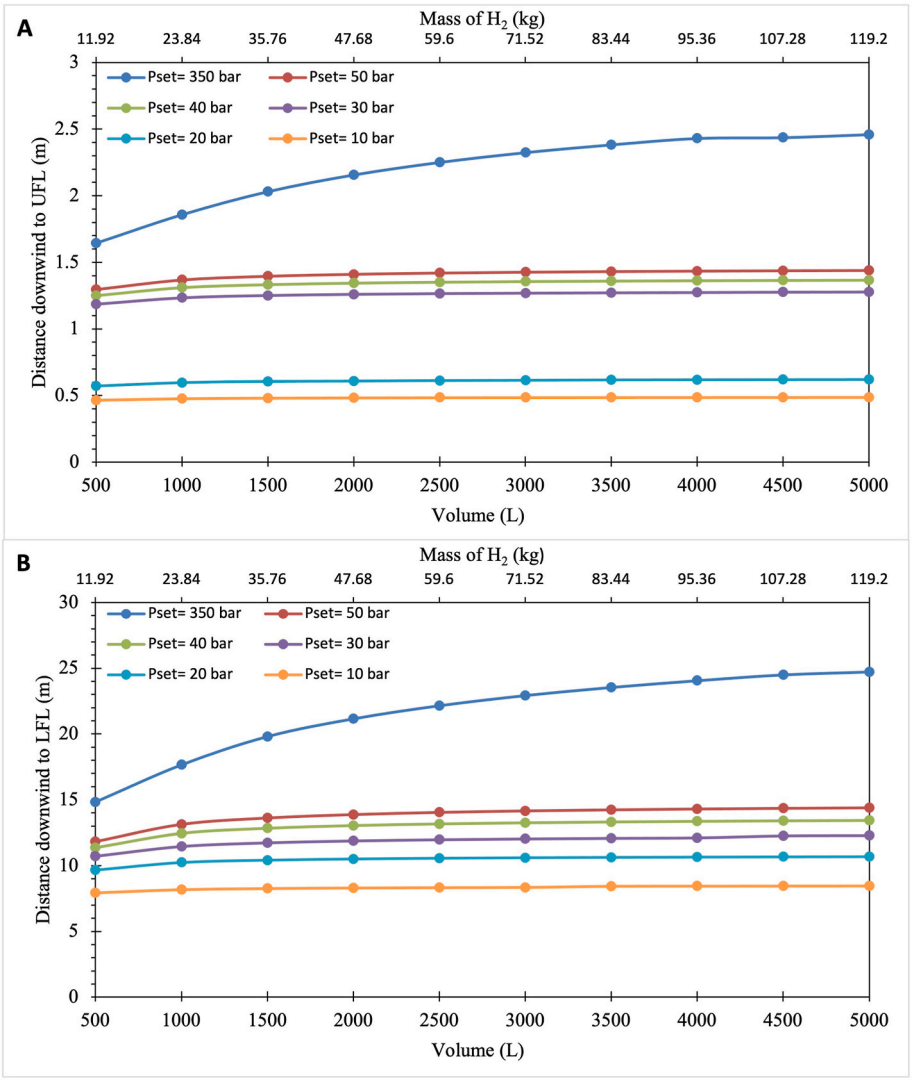

Fig. 3. Continuous release case A) Distance at which the UFL is reached as a function of vessel volume and P_{set}; B) Distance at which the LFL is reached as a function of vessel volume and P_{set}.

Table 4
Distances at which UFL and LFL are reached in the different volumes analyzed and at different P_{set} values.

Volume (L)	350 bar		50 bar		40 bar		30 bar		20 bar		10 bar	
	UFL (m)	LFL (m)	UFL (m)	LFL (m)	UFL (m)	LFL (m)	UFL (m)	LFL (m)	UFL (m)	LFL (m)	UFL (m)	LFL (m)
500	1.64	14.8	1.30	11.8	1.25	11.4	1.18	10.7	0.57	9.6	0.47	7.9
1000	1.85	17.6	1.37	13.1	1.31	12.4	1.23	11.4	0.60	10.2	0.48	8.2
1500	2.03	19.8	1.39	13.6	1.33	12.8	1.25	11.7	0.61	10.4	0.48	8.3
2000	2.16	21.2	1.41	13.9	1.34	13.0	1.26	11.9	0.61	10.5	0.48	8.3
2500	2.25	22.2	1.42	14.0	1.35	13.2	1.27	12.0	0.61	10.6	0.48	8.3
3000	2.32	22.9	1.43	14.2	1.36	13.2	1.27	12.0	0.61	10.6	0.49	8.3
3500	2.38	23.5	1.43	14.2	1.36	13.3	1.27	12.1	0.62	10.6	0.49	8.4
4000	2.43	24.1	1.43	14.3	1.36	13.4	1.27	12.1	0.62	10.6	0.49	8.4
4500	2.44	24.5	1.44	14.3	1.36	13.4	1.28	12.3	0.62	10.7	0.49	8.4
5000	2.46	24.7	1.44	14.4	1.37	13.4	1.28	12.3	0.62	10.7	0.49	8.5

under most conditions. Accordingly, for the fire-induced accidental scenarios analyzed hereafter, a conservative assumption was adopted, whereby hydrogen released from the solution at elevated temperatures is considered fully and promptly available for discharge to the environment (Scenario C).

To provide a clear overview of the decision logic adopted in the safety analysis, a schematic flowchart is introduced in Fig. 2 to summarize the different operating and accidental scenarios considered, the corresponding thermal conditions, and the resulting time-scale-based classification of hydrogen release regimes.

3.2. Dispersion

The hydrogen concentration as a function of the downwind distance from the release point was evaluated using the PHAST 9.0 software, with the objective of quantitatively identifying the zones where the hydrogen

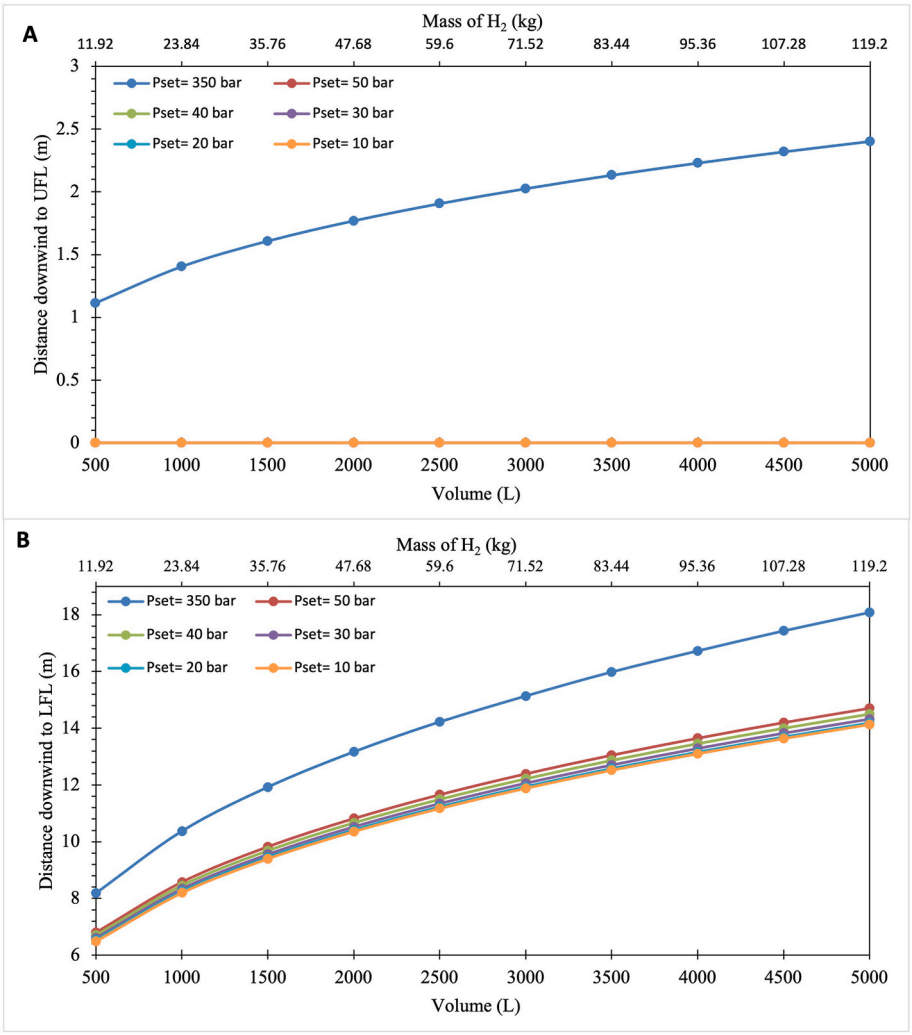

Fig. 4. Catastrophic rupture case. A) Distance at which UFL is reached; B) Distance at which LFL is reached, both as a function of vessel volume and P_{set}.

concentrations fall within the flammable range. The results for continuous hydrogen release at different set pressures P_{set} and tank volumes are reported in Fig. 3.

Fig. 2 shows the downwind distance from the release point at which UFL and LFL are reached, as a function of vessel volume, at different values of P_{set}. Distances are also summarized in Table 4.

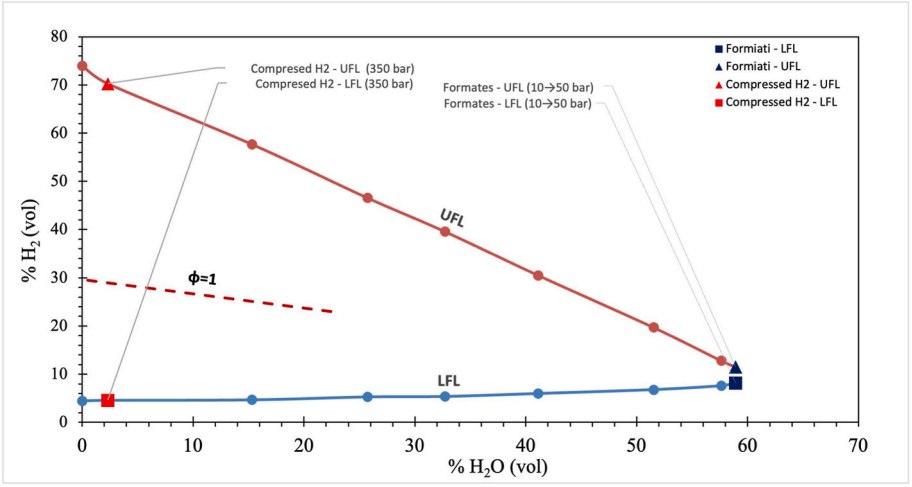

Fig. 5. Flammability envelope (LFL/UFL) of the H_2-steam system (wet base) at fixed T and P. Scenario markers (formate vs. compressed hydrogen) indicate intersections with the limits together with ground-level centerline distances. Fixed inventory across cases: m_{H2} = 199.21 kg; m_{H2O} = 2374.93 kg. Operating assumptions: catastrophic tank rupture (worst-case 5000L), T ambient and atmospheric pressure.

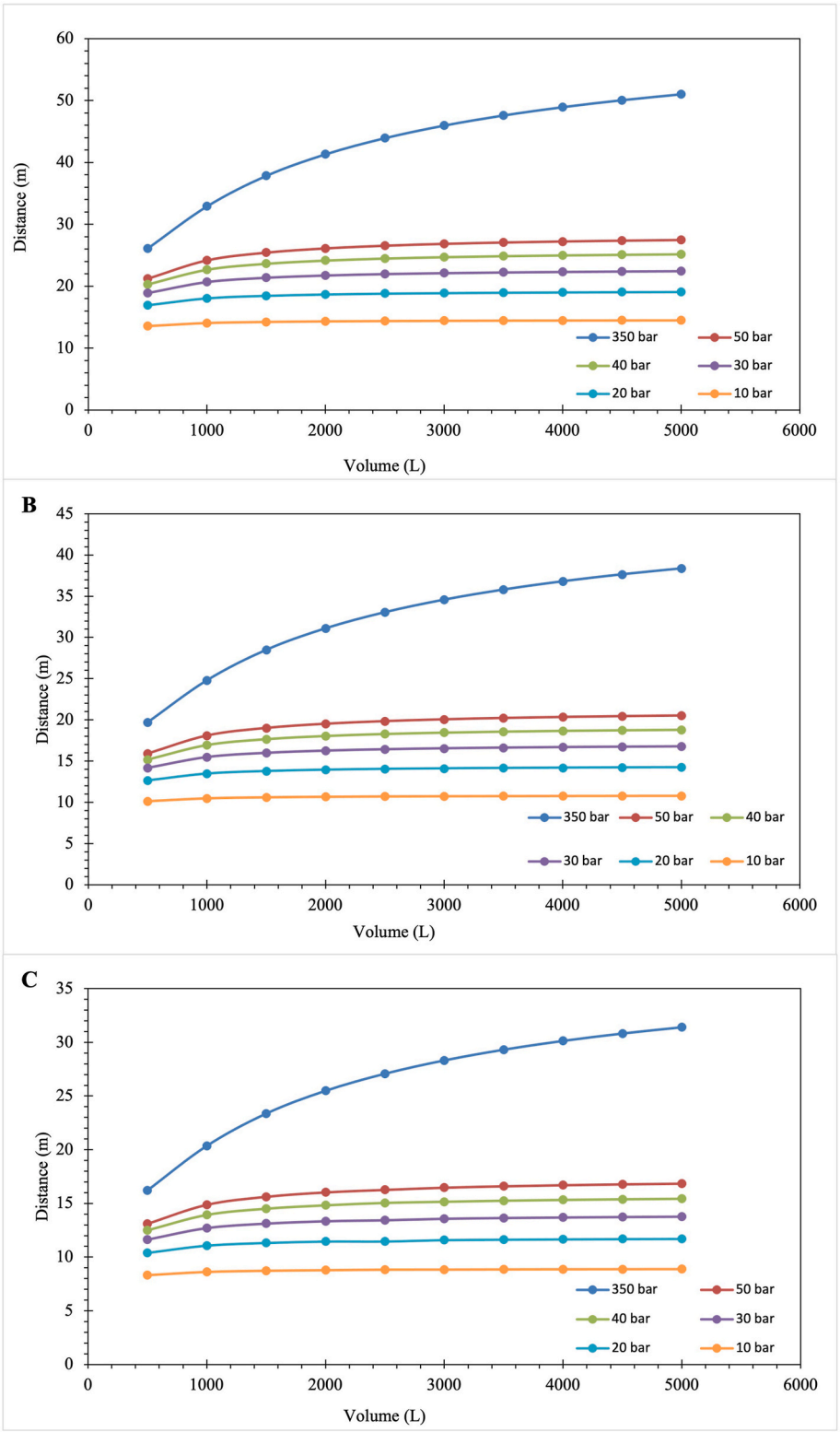

Fig. 6. Distances at which target thermal fluxes (A: 4 kW/m^2; B: 12.5 kW/m^2; C: 37.5 kW/m^2) are reached, for different volumes and P_{set} values.

Adopting a conservative approach, the amount of water vaporizing into the tank headspace is assumed to be negligible compared to the hydrogen. This assumption is supported by thermodynamic calculations. As expected, both the UFL and LFL increase with vessel volume, indicating that larger hydrogen inventories generate broader flammability ranges. Moreover, at higher storage pressures, the affected areas expand further, as larger mass flow rates result in wider hazardous zones. These results highlight the critical role of both vessel size and operating pressure in determining the extent of flammable clouds. Simultaneously with the dispersion analysis, the tank emptying time was estimated using the PHAST *time-varying leak* function, which accounts for the progressive pressure decrease inside the vessel during release. As shown in Fig. S2 (Supplementary Material), lower pressures lead to substantially longer discharge times. For example, at 10 bar, the emptying

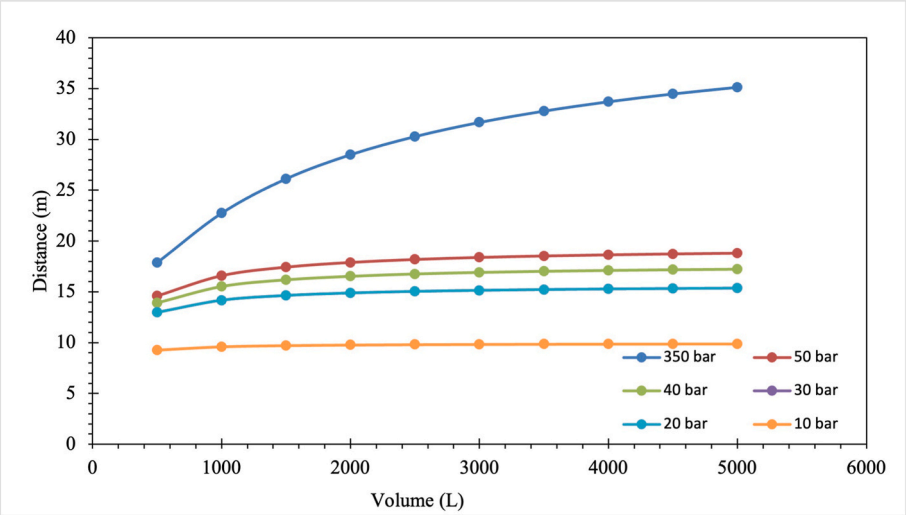

Fig. 7. Distances corresponding to 50% fatality probability, as a function of vessel volume and P_{set}.

duration is approximately fourteen times longer than that associated with compressed gaseous hydrogen storage at 350 bar.

This behavior has relevant safety implications: while low-pressure systems release hydrogen at lower mass flow rates, thereby reducing immediate hazard distances, they sustain the release for much longer times. This extended release could increase the probability of delayed ignition or secondary accident scenarios.

For the instantaneous release scenario, the vessel pressure and temperature rise until catastrophic rapture occurs. The sudden release of water and hydrogen results in instantaneous vaporization of the water and the formation of a puff. In this case, the hydrogen concentration at ground level is above the UFL as soon as the puff is formed, meaning the cloud is essentially over-rich and well mixed. This behavior, observed across all volumes and pressures analyzed, is illustrated in Fig. 4.

This result underlines a mitigating effect of water: in the case of vessels containing aqueous solutions, the hazardous areas associated with hydrogen release are confined closer to the source, thereby limiting the spatial extent of thermal radiation and overpressure effects, as well as the associated fatality and structural damage zones (see Section 3).

Fig. 5 shows the flammability limits of H_2/air mixtures as a function of increasing the water addition. At an H_2O content of 59%, the H_2/air mixture is no longer flammable [57,58].

The figure also reports the actual concentrations corresponding to the case studies investigated in this work, together with the associated centerline distances at ground level. Increasing the vapor fraction progressively narrows the flammable region, ultimately leading to a near-closure condition at approximately 60% relative humidity. At this point, the LFL and UFL converge at an H_2 content of 10%, consistent with values reported in the literature [57,58]. In the formate scenario, the high-water content upon release (steam inerting) positions the mixture directly on the upper branch of the UFL curve at the source. As a result, the release does not exhibit an initial non-flammable, fuel-rich region. As dispersion proceeds, dilution with air decreases the H_2 concentration until it reaches the LFL after short distances (between 14 and 15 m), with limited sensitivity to the tank pressure within the examined inventory range.

In contrast, the compressed-H_2 scenario (representing a dry mixture aside from ambient humidity) exhibits a substantially broader flammable window. The intersection distances with the UFL and LFL (UFL = 2.4 m and LFL = 18.1 m at 350 bar) are correspondingly larger, defining an increased hazard radius for an equivalent inventory. Under constant-inventory conditions, the overlap of the two scenarios on the LFL/UFL curves provides a consistent basis for comparing intrinsic hazard levels. The steam-inerting effect in the formate case restricts the flammable domain and decreases the intersection distances, whereas the dry mixture of compressed hydrogen spans a wider flammability window, resulting in larger downwind distances.

3.3. Consequence analysis

In the continuous release scenario, when the safety valve operates correctly, hydrogen is released staidly. The effect of water vapor remains negligible in this case, either because the amount of steam produced is small compared to hydrogen, or because stratification results in the preferential discharge of hydrogen through the valve. Conversely, in the event of valve malfunction, the vessel pressure rises to the rupture threshold, leading to instantaneous release of a water-hydrogen mixture.

When immediate ignition occurs in the continuous release case, the

Table 5
Average hydrogen mass flow rate and corresponding emptying times calculated using the time-varying leak model.

Volume (L)	Average mass flow rate (kg/s)						Release time (s)					
	350 bar	50 bar	40 bar	30 bar	20 bar	10 bar	350 bar	50 bar	40 bar	30 bar	20 bar	10 bar
500	0.64	0.42	0.38	0.323	0.251	0.156	18	64	75	90	116	172
1000	1.12	0.58	0.50	0.401	0.304	0.168	36	129	149	180	232	344
1500	1.58	0.65	0.55	0.440	0.316	0.172	54	193	224	270	347	516
2000	1.96	0.69	0.58	0.463	0.322	0.174	73	258	299	360	465	689
2500	2.27	0.72	0.60	0.467	0.326	0.176	91	322	373	450	579	861
3000	2.53	0.74	0.611	0.475	0.330	0.177	109	387	448	539	695	1033
3500	2.76	0.75	0.620	0.481	0.333	0.178	127	451	523	629	810	1205
4000	2.95	0.76	0.628	0.485	0.335	0.179	145	516	598	719	926	1377
4500	3.12	0.77	0.634	0.489	0.337	0.179	163	580	672	809	1042	1549
5000	3.27	0.78	0.638	0.491	0.338	0.179	182	645	747	899	1158	1722

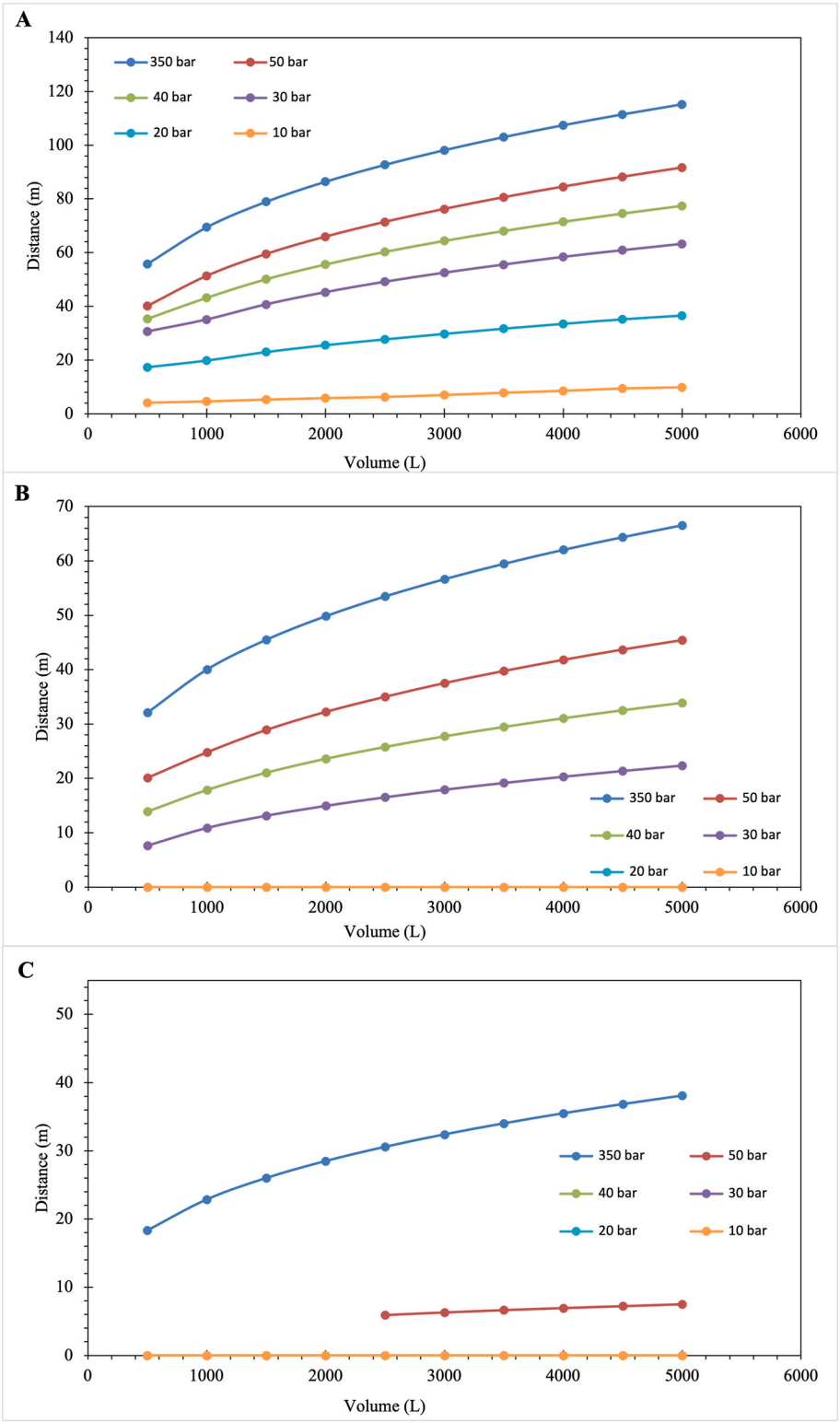

Fig. 8. Distances reached at different thermal flux thresholds (A: 4 kW/m^2; B: 12.5 kW/m^2; C: 37.5 kW/m^2).

most relevant accidental event is the formation of a pressurized hydrogen jet fire. Figs. 6 and 7 report the damage distances for three heat flux thresholds (37.5, 12.5, and 4 kW/m^2) and the corresponding 50% fatality distances, as a function of vessel volume and pressure.

The results clearly show that compressed hydrogen consistently produces larger hazard distances than aqueous storage. Both thermal flux thresholds and fatality distances are significantly more severe at 350 bar across all volumes analyzed. In PHAST simulations, an exposure time of 20 s was assumed, representing a typical average value used in the literature [55].

Interestingly, the increase in damage distance with vessel volume behaves differently depending on the storage pressure. For aqueous formate storage at low pressures, a sharp increase is observed in the 0.5 - 1.5 m^3 range, followed by a plateau at larger volumes. In contrast, for

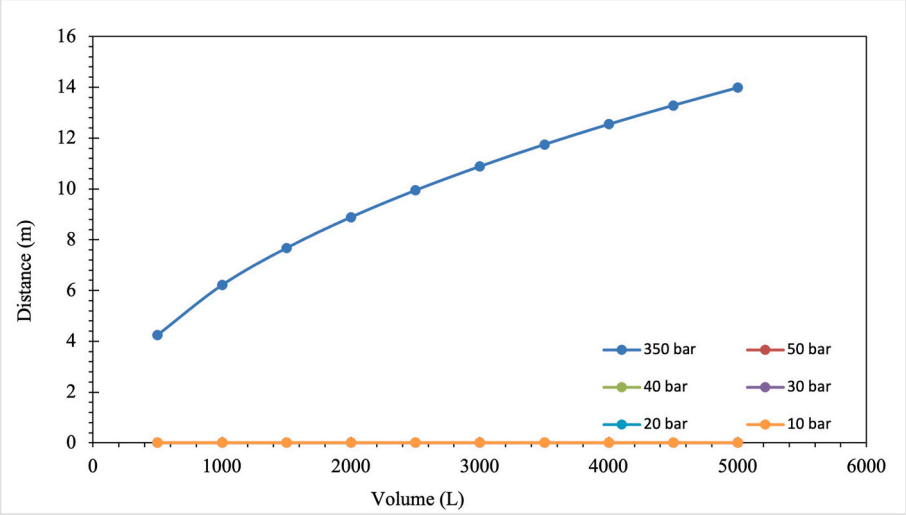

Fig. 9. Distances corresponding to 50% fatalities, as a function of vessel volume and Pset.

compressed hydrogen at 350 bar, the increase remains pronounced throughout the entire volume range. This finding suggests that for high-pressure storage, accident consequences scale directly with vessel size, while for aqueous storage systems the risk escalation is intrinsically limited.

To ensure comparability, all vessel sizes were designed to contain the same hydrogen mass, with storage pressure being the only differentiating parameter. As a result, at higher pressures, the mass flow rate through the valve is significantly greater, as reported in Table 5.

Higher flow rates at elevated pressures produce more energetic jet fires during the early release phase, resulting in longer hazard distances. Conversely, aqueous storage leads to lower outflow rates and less severe consequences, with hazard distances that plateau for large volumes.

When the safety valve fails, vessel rupture occurs once the burst pressure (P_{burst}) is reached. The catastrophic rupture leads to two possible accident scenarios: (i) fireball formation due to immediate ignition of the cloud, and (ii) explosion due to delayed ignition.

For the fireball case, it is important to emphasize that the cloud being formed is diluted by water mixed in the momentum-dominated phase of the physical burst. For the fireball case, simulation results for thermal flux thresholds (37.5, 12.5, 4 kW/m^2) and 50% fatality distances are reported in Figs. 8 and 9.

The graphs illustrate that the impact distances corresponding to different thermal flux thresholds (4, 12.5, and 37.5 kW/m^2) and to the 50% fatality threshold all increase with the vessel volume for every pressure considered. In general, higher storage pressures are associated with longer hazard distances at each intensity level.

As shown in Fig. 8, the effect of storage pressure on hazard distances is evident across all the thermal flux thresholds considered. At higher pressures, greater distances are consistently observed for all vessel sizes, particularly for the 4 kW/m^2 (Figs. 8A) and 12.5 kW/m^2 (Fig. 8B) thresholds. It is noteworthy, however, that at the 12.5 kW/m^2 level, tanks operated at 10 and 20 bar do not reach this thermal flux for any vessel volume. The trend becomes even more pronounced at the highest threshold of 37.5 kW/m^2 (Fig. 8C), where only the 50-bar tank achieves this value, and only for vessel volumes of 2500 L and above. For all other cases, this threshold is never reached.

For the 50% fatality threshold, a similar pattern is observed: damage distances increase with vessel volume and are greatest for compressed hydrogen. In contrast, for aqueous tanks operated at lower pressures, the 50% fatality threshold is never reached within the investigated volume range, as the predicted hazard distances remain zero, even for the largest vessels.

The trends observed in the fireball hazard distances can be explained

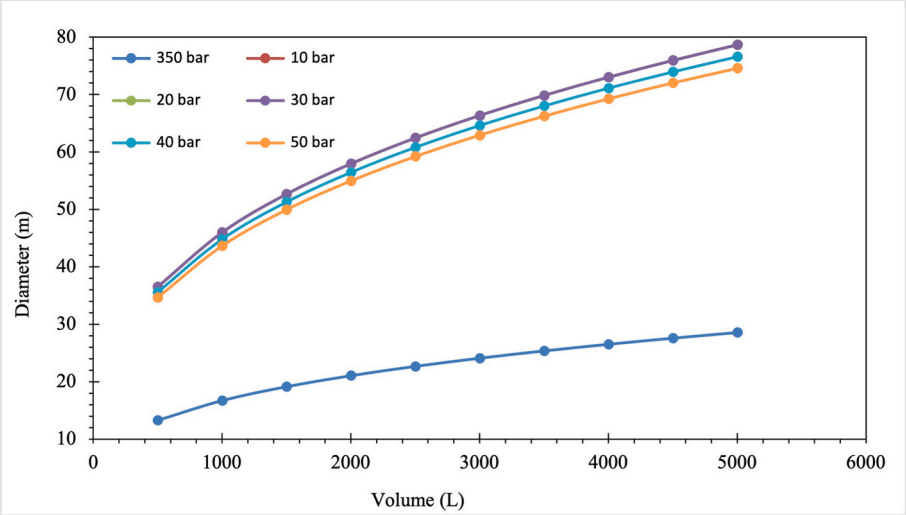

Fig. 10. Fireball diameter generated because of immediate ignition, volume-varying and parametric in P_{set}.

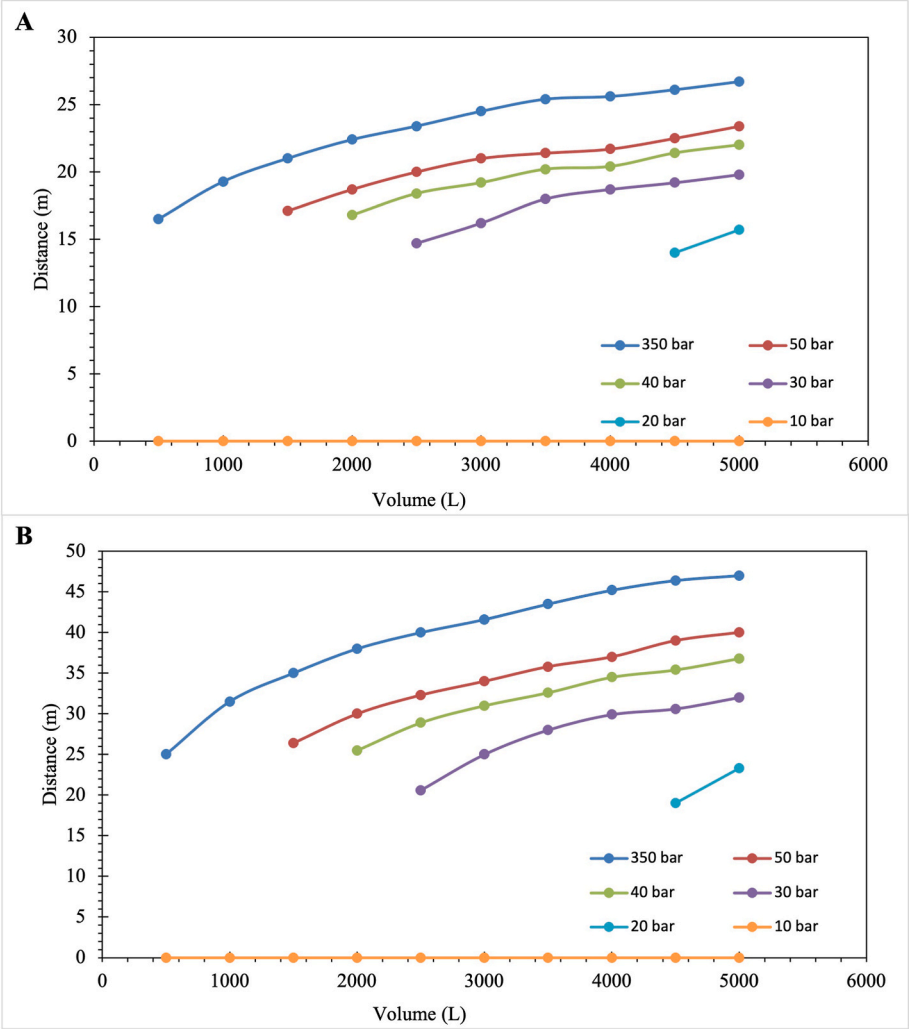

Fig. 11. Distances at which (A) total and (B) 50% destruction of buildings occurs, as a function of vessel volume and parametrized in P_{set}.

by several interconnected physical effects. Pure hydrogen has a lower heating value (HHV) of 12.7 MJ/Nm^3, at standard conditions. When water vapor is present, as in the case of fireball formation from aqueous tanks, hydrogen is diluted, and the available energy per unit volume decreases significantly. This reduction in calorific value directly limits the intensity of the fireball. Moreover, water vapor strongly affects the radiative properties of the fireball: water is an effective absorber and scatterer of thermal radiation, resulting in a marked reduction in radiant efficiency compared to pure hydrogen. Furthermore, Fig. 10, which reports the fireball diameter as a function of vessel volume and pressure, highlights a clear distinction between scenarios. For tanks containing aqueous solutions, fireball diameters are considerably larger and increase with volume, whereas for hydrogen at 350 bar, the fireball diameter remains significantly smaller across all volumes considered.

This effect further contributes to the attenuation of the heat flux transmitted to the surroundings. Another key influence of water vapor is its impact on the fireball size. For the same amount of released hydrogen, the presence of vaporized water produces fireballs up to two or three times larger in diameter than those originating from pure hydrogen tanks, as also shown in Fig. 10. However, this increased fireball volume corresponds to a lower energy density, thereby further reducing the overall hazard.

Together, these effects explain why, for aqueous storage tanks operated at 10-50 bar, the predicted distances for the 50% fatality threshold remain negligible.

Another possible consequence is linked to the explosion of a delayed cloud, resulting in structural damage caused by the overpressure generated. Fig. 11 reports the distances corresponding to 50% destruction of masonry buildings complete destruction of buildings.

As shown in Fig. 11, the damage distance curves for tanks containing aqueous formate solutions consistently lie well below those of compressed hydrogen tanks, across the entire volume range considered. For both 50% and total building destruction thresholds, the distances associated with low-pressure formate solution tanks remain limited, rarely exceeding 20 m even for the largest vessels. By contrast, the curve corresponding to compressed hydrogen at 350 bar display a much steeper increase in damage distance with vessel size, reaching values up to 45 m for total destruction.

Notably, while the curves for formate solution tanks tend to level off at large volumes, indicating a partial saturation effect, whereby increases in vessel size led to only modest extensions of the damage radius, the trend for compressed hydrogen at 350 bar continues to rise sharply throughout the entire investigated volume range. This indicates that, for high-pressure hydrogen storage, both the severity and the extent of accident consequences escalate consistently with increasing vessel size, unlike what is observed for formate solutions at lower pressures.

Additionally, for pressures of 10 and 20 bar, the damage distances are virtually negligible under all conditions, further underscoring the limited risk posed by low-pressure aqueous systems.

It is also worth noting that the presence of water in aqueous formate

Table 6
Radial distances (m) from the catastrophic tank rupture at which the thermal flux thresholds of 4, 12.5, and 37.5 kW/m^2 are reached, as well as the distance corresponding to a 50% probability of fatalities, for different concentration regimes and operating pressures. A dash (-) indicates that the threshold is not reached under the given conditions.

Regime	Analyzed Concentration (mol/L)	Pressure (bar)	4 kW/m^2	12.5 kW/m^2	37.5 kW/m^2	50% fatalities
Diluted (0-6.5)	2	50	-	-	-	-
		40	-	-	-	-
		30	-	-	-	-
		20	-	-	-	-
		10	-	-	-	-
Intermediate (6.5-14)	11.92	50	91.7	45.4	7.5	-
		40	77.5	33.9	-	-
		30	63.3	22.3	-	-
		20	35.5	-	-	-
		10	7	-	-	-
Concentrated (>14)	16	50	161	91	47.6	16
		40	156	87.6	45.4	12.8
		30	149	83.4	42.4	9.6
		20	36.4	-	-	-
		10	7.5	-	-	-

Intrinsically Safe

Possible ignition, no death by thermal flux

Possible ignition, possible death by thermal flux

solutions mitigates the release scenario. Due to its high heat capacity and enthalpy of vaporization, water absorbs a substantial fraction of the released energy, leading to lower overpressure levels compared to the sudden release of pure compressed hydrogen. This inerting effect of water reduces the severity of pressure waves and thus diminishes the potential for structural damage at a given distance.

The main analyses were conducted at a salt concentration of 11.92 mol/L (volumetric energetic density 3.31 MJ/L), which corresponds to an intermediate concentration regime, as defined in Russo et al. [51]. As highlighted in that work, within this concentration range the ignition of the cloud generated by the catastrophic rupture is possible, although it does not produce fatal thermal flux levels. To further support the findings reported in literature, additional simulations were performed under both diluted and concentrated regimes, considering the largest vessel volume as representative of a worst-case scenario in terms of industrial scalability. Table 6 summarizes the results obtained for the three concentration regimes, expressed in terms of the 50% fatality threshold and the corresponding thermal flux levels. A dash (−) indicates that the corresponding threshold is not reached under the given conditions.

3.4. Risk maps

Risk maps and risk transect for a single standard storage vessel with a volume of 5 m^3 in the presence of an external fire were calculated and are summarized in Fig. 12 for unconfined releases. Risk-zone contours were defined as the stand-off distances corresponding to a 50% fatality probability due to the direct consequences of the accidental scenarios. Overall, the use of aqueous formate mixtures for hydrogen storage results in a reduced risk compared with conventional high-pressure storage vessels.

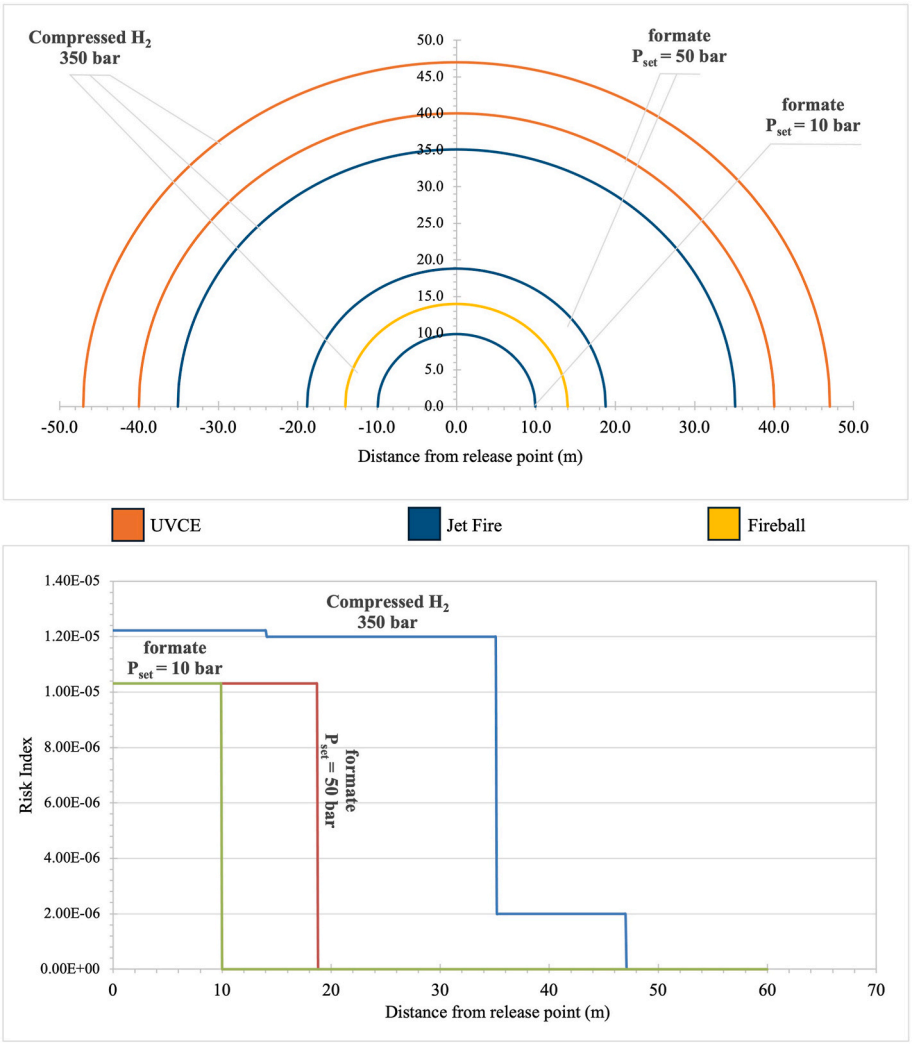

Fig. 12. Risk maps and risk transect for a 5 m^3 storage vessel. Comparison between aqueous formate solution (3.31 MJ/L) and compressed H_2 storage.

4. Conclusions

This study has demonstrated that low-pressure tanks containing aqueous formate solutions present markedly reduced hazardous and lethal consequences for both structures and people compared with conventional high-pressure hydrogen storage systems. The combination of milder operating conditions and the intrinsic presence of water vapor significantly attenuates accident scenarios, even in the most severe case of catastrophic tank rupture.

In fireball scenarios, although the radiated heat flux can reach values of potential concern, its intensity is strongly mitigated by hydrogen dilution within the aqueous mixture, which lowers the effective calorific value. The presence of water further reduces the radiant efficiency of the fireball, limiting both its intensity and hazard distances. The mitigating role of water, acting as an inerting agent through its high heat capacity and enthalpy of vaporization, further reduces the severity of shock waves and their destructive potential.

A key finding of this work is the markedly different scalability behavior of the two storage strategies. While conventional compressed hydrogen storage shows a monotonic increase in accident severity as vessel volume increases, aqueous formate solution tanks display a saturation effect: the scaling-up of tank volumes leads to only modest increments in hazard distances. Furthermore, under accidental release at near-ambient temperature and pressure, hydrogen generation is kinetically limited and concentrations remain below the lower flammability limit, confirming intrinsically safe behavior under normal operating conditions. This characteristic suggests that aqueous formate technologies are not only inherently safer but also more suitable for industrial deployment, since larger storage capacities do not proportionally increase risk levels. From a broader perspective, these results highlight the potential of aqueous formate storage systems as a safer alternative to high-pressure hydrogen, particularly in contexts where safety, urban integration, or public acceptance are critical. The findings also provide useful insights for future design guidelines and regulatory frameworks, supporting the adoption of hydrogen carriers that inherently minimize catastrophic risks while ensuring practical scalability for industrial energy storage applications. It should be noted that the conclusions drawn in this work are based on a comparative assessment between aqueous formate solutions and compressed hydrogen, the latter adopted as a technologically mature and widely implemented benchmark. While alternative storage concepts such as metal hydrides, liquid hydrogen, or solid-state materials are actively investigated, their safety performance is governed by system-specific hydrogen release mechanisms and thermal effects, which were not addressed in the present analysis. Future studies will focus on analyzing the domino effect associated with the release of such solutions, and CFD simulations will be conducted to investigate the degree of mixing between water and hydrogen over longer distances.

CRediT authorship contribution statement

Fabrizio Di Franco: Writing – original draft, Visualization, Software, Methodology, Investigation, Formal analysis, Data curation. **Danilo Russo:** Writing – review & editing, Writing – original draft, Supervision, Project administration, Methodology, Data curation, Conceptualization. **Almerinda di Benedetto:** Writing – review & editing, Supervision, Methodology, Conceptualization.

Declaration of competing interest

The authors declare that they have no known competing financial interests or personal relationships that could have appeared to influence the work reported in this paper.

Acknowledgements

This work was funded by the H2STEM project "Sviluppo di tecnologie e materiali innovativi per lo stoccaggio di idrogeno in fase condensata" (CUP: F57G25000130006), within the framework of the Italian Ministry Environment and Energy Security (MASE), National Recovery and Resilience Plan (PNRR). Investment 3.5 "Research and development on hydrogen", Mission 2 "Green revolution and ecological transition", Component 2 "Renewable energy, hydrogen, grid and sustainable mobility" (M2C2-3.5).

Appendix A. Supplementary data

Supplementary data to this article can be found online at https://doi.org/10.1016/j.ijhydene.2026.154773.

References

[1] Paramati SR, Shahzad U, Doğan B. The role of environmental technology for energy demand and energy efficiency: evidence from OECD countries. Renew Sustain Energy Rev 2022;153:111735. https://doi.org/10.1016/j.rser.2021.111735.
[2] Züttel A, Remhof A, Borgschulte A, Friedrichs O. Hydrogen: the future energy carrier. Philos Trans R Soc A Math Phys Eng Sci 2010;368:3329–42. https://doi.org/10.1098/rsta.2010.0113.
[3] Ornella Kaze. EIA expects U.S. Fossil fuel production to reach new highs in 2023. n.d.
[4] IEA n.d. Global Energy Review: CO2 emissions in 2021. n.d.
[5] Le Quéré C, Andrew RM, Canadell JG, Sitch S, Korsbakken JI, Peters GP, et al. Global Carbon Budget 2016. Earth Syst Sci Data 2016;8:605–49. https://doi.org/10.5194/essd-8-605-2016.
[6] Mensah CN, Long X, Boamah KB, Bediako IA, Dauda L, Salman M. The effect of innovation on CO2 emissions of OCED countries from 1990 to 2014. Environ Sci Pollut Control Ser 2018;25:29678–98. https://doi.org/10.1007/s11356-018-2968-0.
[7] Abdin Z, Zafaranloo A, Rafiee A, Mérida W, Lipiński W, Khalilpour KR. Hydrogen as an energy vector. Renew Sustain Energy Rev 2020;120:109620. https://doi.org/10.1016/j.rser.2019.109620.
[8] Mazloomi K, Gomes C. Hydrogen as an energy carrier: prospects and challenges. Renew Sustain Energy Rev 2012;16:3024–33. https://doi.org/10.1016/j.rser.2012.02.028.
[9] Xu X, Zhou Q, Yu D. The future of hydrogen energy: Bio-hydrogen production technology. Int J Hydrogen Energy 2022;47:33677–98. https://doi.org/10.1016/j.ijhydene.2022.07.261.
[10] Dincer I, Acar C. Innovation in hydrogen production. Int J Hydrogen Energy 2017;42:14843–64. https://doi.org/10.1016/j.ijhydene.2017.04.107.
[11] Ahmed SF, Mofijur M, Nuzhat S, Rafa N, Musharrat A, Lam SS, et al. Sustainable hydrogen production: technological advancements and economic analysis. Int J Hydrogen Energy 2022;47:37227–55. https://doi.org/10.1016/j.ijhydene.2021.12.029.
[12] Navarro RM, Sánchez-Sánchez MC, Alvarez-Galvan MC, Valle F del, Fierro JLG. Hydrogen production from renewable sources: biomass and photocatalytic opportunities. Energy Environ Sci 2009;2:35–54. https://doi.org/10.1039/B808138G.
[13] The EUROPEAN CLEAN hydrogen ALLIANCE reports OF the ALLIANCE ROUNDTABLES ON barriers and MITIGATION measures," 2021. [n.d].
[14] Abe JO, Popoola API, Ajenifuja E, Popoola OM. Hydrogen energy, economy and storage: review and recommendation. Int J Hydrogen Energy 2019;44:15072–86. https://doi.org/10.1016/j.ijhydene.2019.04.068.
[15] Armaroli N, Balzani V. The hydrogen issue. ChemSusChem 2011;4:21–36. https://doi.org/10.1002/cssc.201000182.
[16] Singla MK, Nijhawan P, Oberoi AS. Hydrogen fuel and fuel cell technology for cleaner future: a review. Environ Sci Pollut Control Ser 2021;28:15607–26. https://doi.org/10.1007/s11356-020-12231-8.
[17] Ball M, Wietschel M. The future of hydrogen – opportunities and challenges. Int J Hydrogen Energy 2009;34:615–27. https://doi.org/10.1016/j.ijhydene.2008.11.014.
[18] Rasul MG, Hazrat MA, Sattar MA, Jahirul MI, Shearer MJ. The future of hydrogen: challenges on production, storage and applications. Energy Convers Manag 2022;272:116326. https://doi.org/10.1016/j.enconman.2022.116326.
[19] Yue M, Lambert H, Pahon E, Roche R, Jemei S, Hissel D. Hydrogen energy systems: a critical review of technologies, applications, trends and challenges. Renew Sustain Energy Rev 2021;146:111180. https://doi.org/10.1016/j.rser.2021.111180.
[20] Abdalla AM, Hossain S, Nisfindy OB, Azad AT, Dawood M, Azad AK. Hydrogen production, storage, transportation and key challenges with applications: a review. Energy Convers Manag 2018;165:602–27. https://doi.org/10.1016/j.enconman.2018.03.088.
[21] Barthélémy H. Hydrogen storage – industrial prospectives. Int J Hydrogen Energy 2012;37:17364–72. https://doi.org/10.1016/j.ijhydene.2012.04.121.
[22] Hydrogen lesson learned database [n.d].
[23] Davies E, Ehrmann A, Schwenzfeier-Hellkamp E. Safety of hydrogen storage technologies. Processes 2024;12:2182. https://doi.org/10.3390/pr12102182.
[24] Arsad AZ, Hannan MA, Al-Shetwi AQ, Mansur M, Muttaqi KM, Dong ZY, et al. Hydrogen energy storage integrated hybrid renewable energy systems: a review analysis for future research directions. Int J Hydrogen Energy 2022;47:17285–312. https://doi.org/10.1016/j.ijhydene.2022.03.208.
[25] Le ST, Nguyen TN, Linforth S, Ngo TD. Safety investigation of hydrogen energy storage systems using quantitative risk assessment. Int J Hydrogen Energy 2023;48:2861–75. https://doi.org/10.1016/j.ijhydene.2022.10.082.
[26] Ogbonnaya C, Abeykoon C, Nasser A, Ume CS, Damo UM, Turan A. Engineering risk assessment of photovoltaic-thermal-fuel cell system using classical failure modes, effects and criticality analyses. Clean Environ Syst 2021;2:100021. https://doi.org/10.1016/j.cesys.2021.100021.
[27] Ghosh PC, Emonts B, Janßen H, Mergel J, Stolten D. Ten years of operational experience with a hydrogen-based renewable energy supply system. Sol Energy 2003;75:469–78. https://doi.org/10.1016/j.solener.2003.09.006.
[28] Volken S, Wong-Parodi G, Trutnevyte E. Public awareness and perception of environmental, health and safety risks to electricity generation: an explorative interview study in Switzerland. J Risk Res 2019;22:432–47. https://doi.org/10.1080/13669877.2017.1391320.
[29] Min M, Yoon C, Yoo N, Kim J, Yoon Y, Jung S. Hydrogen risk assessment studies: a review toward environmental sustainability. Energies 2025;18:229. https://doi.org/10.3390/en18020229.
[30] Moradi R, Groth KM. Hydrogen storage and delivery: review of the state of the art technologies and risk and reliability analysis. Int J Hydrogen Energy 2019;44:12254–69. https://doi.org/10.1016/j.ijhydene.2019.03.041.
[31] Wang X, Li B, Han B, Jin X, Zhang D, Bi M. Explosion of high pressure hydrogen tank in fire: mechanism, criterion, and consequence assessment. J Energy Storage 2023;72:108455. https://doi.org/10.1016/j.est.2023.108455.
[32] Liu B, Li Y, Ma Y, Wang L. Electrostatic characteristics analysis and risk assessments of liquid hydrogen storage system. Int J Hydrogen Energy 2024;55:1322–34. https://doi.org/10.1016/j.ijhydene.2023.12.036.
[33] Groth KM, Hecht ES. HyRAM: a methodology and toolkit for quantitative risk assessment of hydrogen systems. Int J Hydrogen Energy 2017;42:7485–93. https://doi.org/10.1016/j.ijhydene.2016.07.002.
[34] Dadashzadeh M, Kashkarov S, Makarov D, Molkov V. Risk assessment methodology for onboard hydrogen storage. Int J Hydrogen Energy 2018;43:6462–75. https://doi.org/10.1016/j.ijhydene.2018.01.195.
[35] Kim J, Lee Y, Moon I. An index-based risk assessment model for hydrogen infrastructure. Int J Hydrogen Energy 2011;36:6387–98. https://doi.org/10.1016/j.ijhydene.2011.02.127.
[36] Ba Q, Zhao Z, Zhang Y, Liu Y, Christopher DM, Ge P, et al. Modeling of cryogenic compressed hydrogen jet flames. Int J Hydrogen Energy 2024;51:917–27. https://doi.org/10.1016/j.ijhydene.2023.06.265.
[37] Klopčič N, Grimmer I, Winkler F, Sartory M, Trattner A. A review on metal hydride materials for hydrogen storage. J Energy Storage 2023;72:108456. https://doi.org/10.1016/j.est.2023.108456.
[38] Rusman NAA, Dahari M. A review on the current progress of metal hydrides material for solid-state hydrogen storage applications. Int J Hydrogen Energy 2016;41:12108–26. https://doi.org/10.1016/j.ijhydene.2016.05.244.
[39] Modisha PM, Ouma CNM, Garidzirai R, Wasserscheid P, Bessarabov D. The prospect of hydrogen storage using liquid organic hydrogen carriers. Energy & Fuels 2019;33:2778–96. https://doi.org/10.1021/acs.energyfuels.9b00296.
[40] Le T-H, Tran N, Lee H-J. Development of liquid organic hydrogen carriers for hydrogen storage and transport. Int J Mol Sci 2024;25:1359. https://doi.org/10.3390/ijms25021359.
[41] Makaryan IA, Sedov IV, Maksimov AL. Hydrogen storage using liquid organic carriers. Russ J Appl Chem 2020;93:1815–30. https://doi.org/10.1134/S1070427220120034.
[42] Langmi HW, Ren J, North B, Mathe M, Bessarabov D. Hydrogen storage in metal-organic frameworks: a review. Electrochim Acta 2014;128:368–92. https://doi.org/10.1016/j.electacta.2013.10.190.
[43] Zhang X, Liu P, Zhang Y. The application of MOFs for hydrogen storage. Inorg Chim Acta 2023;557:121683. https://doi.org/10.1016/j.ica.2023.121683.

[44] Chen Z, Kirlikovali KO, Idrees KB, Wasson MC, Farha OK. Porous materials for hydrogen storage. Chem 2022;8:693–716. https://doi.org/10.1016/j.chempr.2022.01.012.
[45] Mahmoud LAM, Rowlandson JL, Fermin DJ, Ting VP, Nayak S. Porous carbons: a class of nanomaterials for efficient adsorption-based hydrogen storage. RSC Applied Interfaces 2025;2:25–55. https://doi.org/10.1039/D4LF00215F.
[46] Yüksel Alpaydın C, Colpan CO, Karaoğlan MU, Karahan Gülbay S. A comparison of the effects of sodium borohydride-based hydrogen storage System and compressed hydrogen storage tank on the fuel cell vehicle performance. J Energy Resour Technol 2021;143. https://doi.org/10.1115/1.4052163.
[47] Laalam A, Bazazi P. Holding the invisible: advanced materials for hydrogen storage. Int J Hydrogen Energy 2025;169:151057. https://doi.org/10.1016/j.ijhydene.2025.151057.
[48] Russo D, Calabrese M, Marotta R, Andreozzi R, Di Benedetto A. Thermodynamics of the cyclic formate/bicarbonate interconversion for hydrogen storage. Int J Hydrogen Energy 2022;47:31370–80. https://doi.org/10.1016/j.ijhydene.2022.07.033.
[49] Calabrese M, Russo D, di Benedetto A, Marotta R, Andreozzi R. Formate/bicarbonate interconversion for safe hydrogen storage: a review. Renew Sustain Energy Rev 2023;173:113102. https://doi.org/10.1016/j.rser.2022.113102.
[50] Bahuguna A, Sasson Y. Formate-Bicarbonate cycle as a vehicle for hydrogen and energy storage. ChemSusChem 2021;14:1258–83. https://doi.org/10.1002/cssc.202002433.
[51] Russo D, Andreozzi R, Calabrese M, Marotta R, Di Benedetto A. Quantitative risk assessment of aqueous formate for hydrogen storage. Int J Hydrogen Energy 2024;65:421–7. https://doi.org/10.1016/j.ijhydene.2024.04.069.
[52] Makridis SS. Hydrogen storage and compression. Methane and hydrogen for Energy Storage. Institution of Engineering and Technology; 2016. p. 1–28. https://doi.org/10.1049/PBPO101E_ch1.
[53] Micheal Hirscher. Handbook of hydrogen storage: new materials for future energy storage. n.d.
[54] Han S, Baek S-H, Jeon Y, Kim K, Park S. Integrated experimental-computational approach to estimate TNT equivalence of hydrogen vessel bursts. Int J Hydrogen Energy 2025;146:149936. https://doi.org/10.1016/j.ijhydene.2025.06.126.
[55] Froeling HAJ, Dröge MT, Nane GF, Van Wijk AJM. Quantitative risk analysis of a hazardous jet fire event for hydrogen transport in natural gas transmission pipelines. Int J Hydrogen Energy 2021;46:10411–22. https://doi.org/10.1016/j.ijhydene.2020.11.248.
[56] Dong Z, Mukhtar A, Ludwig T, Akhade SA, Hu W, Hu JZ, et al. Silver-decorated palladium on carbon catalyst for enhanced ammonium formate dehydrogenation. Catal Sci Technol 2024;14:449–63. https://doi.org/10.1039/D3CY01057K.
[57] Shapiro ZM, Moffette TR. Hydrogen flammability data and application to PWR loss-of-coolant accident. 1957.
[58] Marshall BW, Hydrogen J, Air. Steam flammability limits and combustion characteristics in the FITS vessel. 1986.